

Attosecond time delay in valence photoionization and photorecombination of argon: A time-dependent local-density-approximation study

Maia Magrakvelidze,¹ Mohamed El-Amine Madjet,² Gopal Dixit,³ Misha Ivanov,^{3,4} and Himadri S. Chakraborty^{1,*}

¹*Department of Natural Sciences, D.L. Hubbard Center for Innovation and Entrepreneurship, Northwest Missouri State University, Maryville, Missouri 64468, USA*

²*Qatar Environment and Energy Research Institute, Qatar Foundation, P.O. Box 5825, Doha, Qatar*

³*Max Born Institute, Max-Born-Strasse 2A, 12489 Berlin, Germany*

⁴*Blackett Laboratory, Imperial College London, London SW7 2AZ, United Kingdom*

(Received 20 November 2014; published 22 June 2015)

We determine and analyze the quantum phases and time delays in photoionization and photorecombination of valence $3p$ and $3s$ electrons of argon using the Kohn-Sham local-density-functional approach. The time-dependent local-density approximation is used to account for the electron correlation. Resulting attosecond Wigner-Smith time delays show very good agreement with the recent experiment on argon that measured the delay in $3p$ photorecombination [S. B. Schoun *et al.*, *Phys. Rev. Lett.* **112**, 153002 (2014)].

DOI: [10.1103/PhysRevA.91.063415](https://doi.org/10.1103/PhysRevA.91.063415)

PACS number(s): 32.80.Fb, 31.15.E–

I. INTRODUCTION

Technological advances in producing the isolated attosecond pulse [1,2] and attosecond pulse trains [3,4] have facilitated pump-probe experiments to resolve the photoionization (PI) process in real time [5–9]. In attosecond streaking measurements, following the ionization by an extreme ultraviolet (XUV) pump pulse, photoelectrons are boosted by the infrared (IR) probe vector potential to different final momenta as a function of pump-probe time delay, which are then mapped into a spectrogram. Theoretical modeling of such spectrograms extracts the time delay associated with PI. For instance, the relative time delay between photoelectrons emitted from $2s$ and $2p$ orbitals of atomic neon [5] and that between photoelectrons from conduction and valence bands in bulk metals have been measured using streaking methods [8,9]. By introducing a coincidence technique of photoelectron detection, multiple streaking traces can be determined in a single experiment for emissions from various atomic orbitals or from different gas species in a mixed sample [10]. In the interferometric measurements, namely, reconstruction of attosecond beating by interference of two-photon transitions (RABITT) [3], photoelectrons emitted by odd harmonics of an XUV pulse train subsequently absorb or emit an IR photon. This produces even harmonic sidebands in the spectrogram. The ionization time delay is then obtained by the ratio of the difference of the measured phases at consecutive sidebands and the harmonic separation. Important recent measurements using the RABITT technique include relative delay between argon $3s$ and $3p$ photoemission [6,7] and between emissions from various noble-gas atoms [11].

The additional delay introduced by the IR probe pulse via the so-called continuum-continuum coupling or Coulomb-laser coupling can be calculated separately and subtracted from the measured result, yielding the Wigner-Smith delay associated with PI [12–14]. This is because the phase-frequency difference approach mentioned above approximates

the energy differential of the phase of the PI amplitude that defines the Wigner-Smith delay [15,16]. This delay is the excess time, positive or negative, spent by the electron to reach the continuum in addition to the time it would take in the absence of interactions between the continuum electron and the target. Therefore, attosecond time delay is an important probe of dynamical correlation effects in PI processes. Several theoretical methods employed to explain experimental $3s$ - $3p$ relative delay in argon were only partially successful to reproduce measurements [6,7,17–20], with the exception of the multiconfigurational Hartree-Fock method, which had better success [21].

Recently, the phase and the group delay associated with photorecombination (PR) of the argon $3p$ electron at energies that include the $3p$ Cooper minimum have been measured using the combination of high-harmonic generation (HHG) and RABITT methods [22]. Observations of the Cooper minima in HHG spectra of various atoms and molecules have been a subject of recent work [23–28]. The presence of such minima in HHG spectra indicates that the structure of the sample can be probed despite the presence of a strong IR pulse during recombination. The assumption of time-reversal symmetry between PR and PI forms the basis of the principle of detailed balance [29]. This leads to a one-to-one correspondence between PR and PI [30,31], which permits the retrieval of structural and dynamical information of the sample from HHG spectra.

The purpose of the present paper is to provide a detailed theoretical analysis of the phase and Wigner-Smith time delay associated with PI and PR processes. We report the calculation of these phases and delays for argon using the time-dependent local-density approximation (TDLDA) method and show that the results successfully describe recent PR [22] measurements. The argon atom is one of the most studied systems for HHG and attosecond pulse generation and has a $3s$ and a $3p$ Cooper minimum at, respectively, 42- and 48-eV photon energy in the PI cross section [32,33] [the latter yields a (53 ± 3) -eV minimum in the HHG spectra [23–25]]. Our study highlights the importance of the second dipole-allowed channel at energies near the Cooper minimum of a given channel with the

*himadri@nwmissouri.edu

same initial orbital and, in general, stresses the applicability of the TDLDA method to interpret RABITT measurements. Results also add reliability to recent TDLDA predictions [19,34,35] of the PI time delay in fullerene materials.

This paper is structured as follows. Section II includes three subsections: Sec. II A describes PI and PR within the independent-particle model, i.e., the local-density approximation (LDA); Sec. II B provides the essentials of the TDLDA, which incorporates important electron-electron correlations; and Sec. II C gives an alternative discussion about the electron correlation in PI and PR via the interchannel coupling formalism by Fano. Section III discusses numerical results and their comparison with recent measurements. A summary is presented in Sec. IV.

II. THEORETICAL PERSPECTIVES

A. Independent-particle model

Choosing the photon polarization along the z axis, the PI and PR dipole transition amplitudes in a single-channel approximation, which omits electron correlations, are

$$d_{\text{PI}}(\mathbf{k}) = \langle \psi_{\mathbf{k}l'}^- | z | \phi_{nl} \rangle \quad (1a)$$

and

$$d_{\text{PR}}(-\mathbf{k}) = \langle \phi_{nl} | z | \psi_{-\mathbf{k}l'}^+ \rangle. \quad (1b)$$

Here k is the momentum of the continuum electron, z is the one-body dipole operator, ϕ_{nl} is the bound wave function of the target, and $\psi_{\mathbf{k}l'}$, with $+$ ($-$) representing the outgoing (incoming) spherical continuum wave function, is

$$\psi_{\mathbf{k}l'}^\pm(\mathbf{r}) = (8\pi)^{3/2} \sum_m e^{\pm i\eta_{l'}} R_{kl'}(r) Y_{l'm}(\Omega_{\mathbf{r}}) Y_{l'm}^*(\Omega_{\mathbf{k}}), \quad (2)$$

with $l' = l \pm 1$. In Eq. (2), the scattering phase $\eta_{l'}(k)$ contains contributions from both short-range and Coulomb potentials and $R_{kl'}$ is the radial continuum wave. Since $(\psi_{-\mathbf{k}}^+)^* = \psi_{\mathbf{k}}^-$, it follows from Eqs. (1) that $d_{\text{PI}} = d_{\text{PR}}$, satisfying the time-reversal symmetry between PI and PR.

We calculate amplitudes d [Eqs. (1)] using the independent-particle LDA method [36–38]. Here the LDA potential, using the single-particle density $\rho(\mathbf{r})$,

$$V_{\text{LDA}}(\mathbf{r}) = -\frac{z}{r} + \int d\mathbf{r}' \frac{\rho(\mathbf{r}')}{|\mathbf{r} - \mathbf{r}'|} + V_{\text{XC}}[\rho(\mathbf{r})], \quad (3)$$

uses the Leeuwen-Baerends exchange-correlation functional V_{XC} [39], which provides an accurate asymptotic description of the ground-state potential. The LDA self-consistently includes an average interaction with the ionic core and obtains the ground and continuum single-electron states for various angular momenta in a mean-field approximation. Thus, the LDA is akin to the Hartree-Fock method, albeit an approximation to the (nonlocal) exchange in a local frame.

We note the following in our LDA results. The absolute value of the amplitude $|d|$ of PI and PR dipole channels $3p \leftrightarrow kd$ shows minima at an energy of about 37 eV, below the energy of the regular $3p$ Cooper minimum. In Fig. 2(a), such a minimum in the $3p \rightarrow kd$ LDA cross section is seen, but no minimum is found in $3s \rightarrow kp$. Equations (1) include LDA radial matrix elements $\langle R_{kd,ks} | z | R_{3p} \rangle$ and $\langle R_{3p} | z | R_{kd,ks} \rangle$,

respectively, for PI and PR. The scattering phase [η in Eq. (2)] of PI and PR does not have any structure at these energies. As the radial matrix element associated with the $3p \rightarrow kd$ transition changes its sign, the total phase corresponding to the total matrix element has a sharp and discontinuous phase jump at the Cooper minimum, which is at a lower energy compared to the experimentally observed minimum. Note that only the scattering phase is considered at the mean-field approximation and our LDA results (not shown) are consistent with the Hartree-Fock results for argon PI [18,40]. We show below that when the electron correlation is included via the complex induced potential in the TDLDA [see Eq. (4)], the position of the Cooper minimum in the cross section and the variation of the total phase of the radial matrix element at the Cooper minimum reproduce the measured results.

B. Time-dependent local-density approximation

The TDLDA, used here to calculate the full transition amplitude, includes many-electron effects and utilizes the advanced G^+ (for PI) and retarded G^- (for PR) Green's functions [37,41,42]. In a linear response frame, such as the TDLDA, the PI and PR amplitudes formally read

$$D_{\text{PI}}(\mathbf{k}) = \langle \psi_{\mathbf{k}l'}^- | \delta V_+^* + z | \phi_{nl} \rangle = d_{\text{PI}}(\mathbf{k}) + \langle \delta V_+^* \rangle \quad (4a)$$

and

$$D_{\text{PR}}(-\mathbf{k}) = \langle \phi_{nl} | z + \delta V_- | \psi_{-\mathbf{k}l'}^+ \rangle = d_{\text{PR}}(-\mathbf{k}) + \langle \delta V_- \rangle. \quad (4b)$$

Here δV_\pm are complex induced potentials that account for electron correlations. In the TDLDA, $z + \delta V_\pm$ are proportional to the induced frequency-dependent changes in the electron density [43]. This change is

$$\delta\rho_\pm(\mathbf{r}'; \omega) = \int \chi_\pm(\mathbf{r}, \mathbf{r}'; \omega) z d\mathbf{r}, \quad (5)$$

where the full susceptibility χ builds the dynamical correlation from the independent-particle LDA susceptibilities

$$\begin{aligned} \chi_\pm^0(\mathbf{r}, \mathbf{r}'; \omega) &= \sum_{nl}^{\text{occ}} \phi_{nl}^*(\mathbf{r}) \phi_{nl}(\mathbf{r}') G^{(\pm)}(\mathbf{r}, \mathbf{r}'; \epsilon_{nl} + \omega) \\ &+ \sum_{nl}^{\text{occ}} \phi_{nl}(\mathbf{r}) \phi_{nl}^*(\mathbf{r}') G^{(\pm)*}(\mathbf{r}, \mathbf{r}'; \epsilon_{nl} - \omega) \end{aligned} \quad (6)$$

via the matrix equation $\chi = \chi^0 [1 - (\partial V / \partial \rho) \chi^0]^{-1}$ involving the variation of the ground-state potential V with respect to the ground-state density ρ . The radial components of the full Green's functions in Eq. (6) are constructed with the regular f_L and irregular g_L solutions of the homogeneous radial equation

$$\left(\frac{1}{r^2} \frac{\partial}{\partial r} r^2 \frac{\partial}{\partial r} - \frac{L(L+1)}{r^2} - V_{\text{LDA}} + E \right) f_L(g_L)(r; E) = 0 \quad (7)$$

as

$$G_L^\pm(r, r'; E) = \frac{2f_L(r_{<}; E)h_L^{(\pm)}(r_{>}; E)}{W[f_L, h_L]}, \quad (8)$$

where W represents the Wronskian and $h_L^{(\pm)} = g_L \pm i f_L$ are complex conjugate combinations. Obviously, the latter fact, along with Eqs. (5)–(8), demonstrates that $\delta V_+^* = \delta V_-$, thus

confirming $D_{PI} = D_{PR}$. Note that the TDLDA thus includes the dynamical correlation by improving upon the mean-field LDA basis. The numerical results presented in this paper are obtained using the TDLDA method only.

C. Electron correlations via interchannel coupling

Before discussing our numerical results, we present the Fano formalism of interchannel coupling, which is used to interpret the results. For photon energies of current interest, the dominant correlation emerges between valence $3p$ and $3s$ channels, since argon's inner electrons are too deeply bound. An elegant way to interpret the dynamical correlation is through the coupling between independent-particle channels as described by Fano [44]. For instance, in the first-order perturbation theory, to approximate the exact continuum wave function of the $3p \rightarrow kd$ channel, coupled to the degenerate $3s \rightarrow kp$ (perturbing) channel, we obtain for the corrected wave function

$$\begin{aligned} |\Psi_{kd}^-(E)\rangle &= |\psi_{kd}^-\rangle + \lim_{\lambda \rightarrow 0} \int dE' \frac{\langle \tilde{\psi}_{kd}^- | 1/r_{12} | \tilde{\psi}_{kp}^- \rangle}{E - E' + i\lambda} |\psi_{kp}^-\rangle \\ &\approx |\psi_{kd}^-\rangle + c \langle \tilde{\psi}_{kd}^- | \frac{1}{r_{12}} | \tilde{\psi}_{kp}^- \rangle |\psi_{kp}^-\rangle. \end{aligned} \quad (9)$$

Here $\tilde{\psi}$ are two-electron wave functions that include both bound and continuum states of an independent-particle channel and c is a complex number that includes the contributions of pole and principal value terms, both accumulated near $E' = E$. In the second step above, we approximate the energy integral by the leading contribution at $E' = E = k^2/2$ for simplicity. Using Eq. (9) in the form (1a), the correlation-corrected PI amplitude can be written as

$$D_{3p \rightarrow kd} = \langle \Psi_{kd}^- | z | \phi_{3p} \rangle = d_{3p \rightarrow kd} + c \langle \tilde{\psi}_{kp}^- | \frac{1}{r_{12}} | \tilde{\psi}_{kd}^- \rangle d_{3s \rightarrow kp}, \quad (10)$$

in which the complex interchannel coupling matrix element $\langle 1/r_{12} \rangle$ with a two-body operator embodies the fraction of the independent-particle $3s \rightarrow kp$ strength that transfers, via correlation, to the observed $3p \rightarrow kd$ channel. Note that, since both bound and continuum wave functions constitute $\tilde{\psi}$, this correlation incorporates the continuum-continuum interaction between the detected d and perturbing p photoelectrons augmented by the strong $3p$ - $3s$ bound-state overlap. Specifically, the correlation is expected to dominate the Cooper-minimum region where the strength of the observing channel is small. Figure 1(a) is a phenomenological representation of Eq. (10) for the detection of $3p$ electrons where the vertical arrows denote independent-particle PIs and the curved arrow is the $3s$ -to- $3p$ correlation contribution.

The corresponding time-reversed photoamplitude with interchannel coupling, plugging the outgoing version of Eq. (9) in the form (1b), can likewise be found as

$$\begin{aligned} D_{3p \leftarrow kd} &= \langle \phi_{3p} | z | \Psi_{kd}^+ \rangle \\ &= d_{3p \leftarrow kd} + c^* \langle \tilde{\psi}_{kd}^+ | \frac{1}{r_{12}} | \tilde{\psi}_{kp}^+ \rangle d_{3s \leftarrow kp}, \end{aligned} \quad (11)$$

which is sketched in Fig. 1(b) and can be shown to exactly equal to its time-forward counterpart (10) since $(\tilde{\psi}_{-k}^+)^* = \tilde{\psi}_{k}^-$

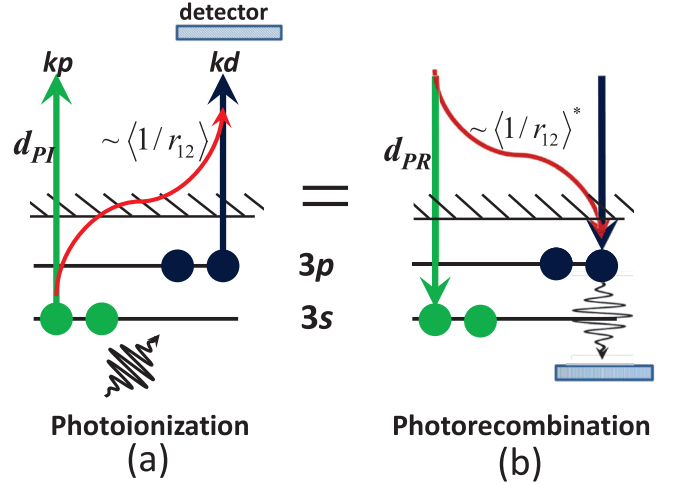


FIG. 1. (Color online) Schematics of total photoamplitudes for transitions of the $3p$ electron. Vertical arrows are single-channel matrix elements for $3p$ and $3s$ [Eqs. (1)], while curved arrows represent the coupling via the interchannel matrix elements $\langle 1/r_{12} \rangle$ [see the text after Eq. (10)]. The detector in each panel identifies the channel being observed in this two-channel interaction model.

and $d_{PI} = d_{PR}$. Obviously, Eq. (11) or Fig. 1(b) is the $3p \leftarrow kd$ PR process correlation modified by its coupling with $3s \leftarrow kp$. One can likewise show the equality of PI versus PR amplitudes by choosing to observe the $3s$ channel that couples to a $3p$ channel.

Note that the correlation expressed in the wave function via the interchannel coupling in Eq. (9) effectively reincarnates in the operator δV in Eqs. (4). In fact, $\langle \delta V \rangle$ corresponds to the correlation contribution in Eq. (10) [45].

III. RESULTS, DISCUSSION, AND COMPARISON WITH MEASUREMENTS

The total, $3p$, and $3s$ PI cross sections for argon, obtained within the TDLDA, are in very good agreement with the measurements [32,33] as shown previously by us [19]. The PR cross sections are derivable directly from PI results by incorporating the principle of detailed balance. The TDLDA phase Γ of the amplitude D is the sum of the LDA phase $l'\frac{\pi}{2} + \eta$ [Eq. (2)] and the phase (the correlation phase) of the complex radial matrix element embedded in D . These phases for channels involving $3p$ and $3s$ electrons are shown in Fig. 2(b). At energies directly above the ionization thresholds, η is dominated by the Coulomb phase. The phases of $3s \rightarrow kp$ and $3p \rightarrow kd$ exhibit rapid variations at their respective Cooper minima at 42 and 48 eV. These minima are also seen in the TDLDA cross sections for PI in Fig. 2(a). Evidently, the correlation blueshifts the $3p$ Cooper minimum from its LDA position (37 eV). The correlation now also introduces a phase variation at the zero of $\text{Re}(D)$, since D is now complex due to the complex δV in Eq. (4a). In the Fano formalism, the nontrivial origin of this complex D is the interchannel coupling matrix element in Eq. (10).

Further, for the $3s$ ionization, one rewrites Eq. (10) for $3s \rightarrow kp$ modified by the coupling with $3p \rightarrow kd$; this entails the d on the right-hand side to interchange and the interchannel

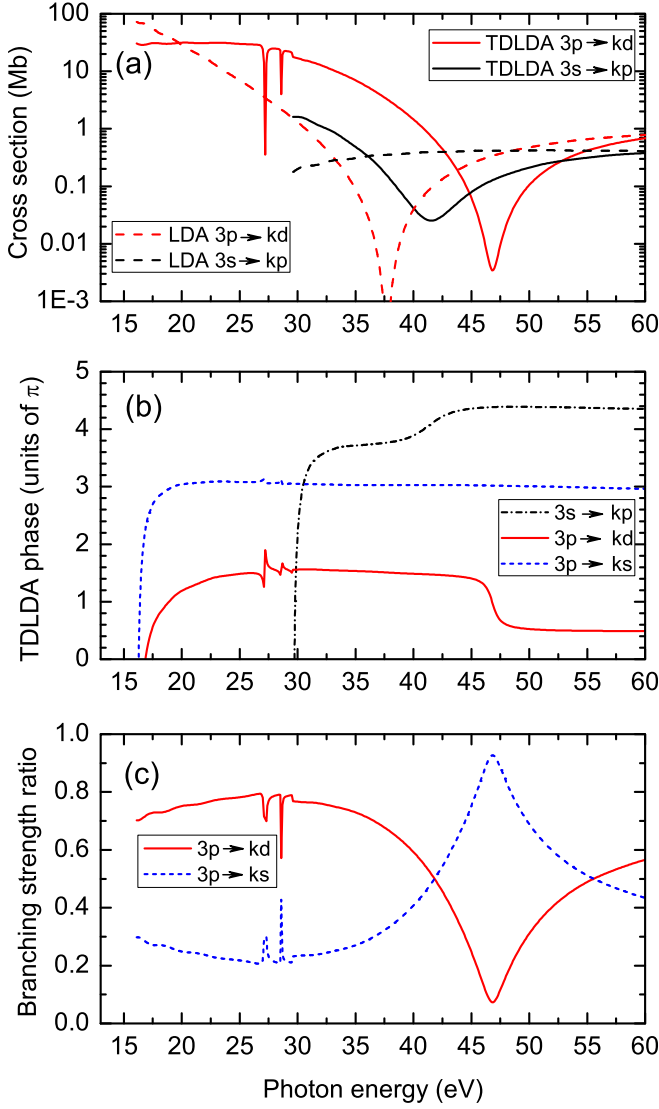


FIG. 2. (Color online) (a) The LDA and TDLDA cross sections for $3p \rightarrow kd$ and $3s \rightarrow kp$ photoionization channels. (b) The TDLDA phases for $3p \rightarrow kd, ks$ channels. Structures between 25 and 30 eV in $3p$ curves are from $3s$ excitations Rydberg resonances. (c) Branching strength ratios [see Eq. (14)] are used in weighted averaging the phases of two dipole channels of $3p$ electrons.

coupling matrix element to conjugate. Two important consequences emerge: (i) The coupling term now directly inserts a minimum in the TDLDA $3s$ channel [Fig. 2(b)] via the LDA amplitude d of $3p \rightarrow kd$ that has a minimum and is stronger enough than the $3s$ channel to dramatically modify it through the interchannel coupling and (ii) the complex conjugation of the interchannel coupling matrix element explains why there are opposite variations in $3p$ and $3s$ phases at their respective minima in Fig. 2(b). A similar relative trend is also found by the random-phase approximation with exchange (RPAE) [18]. The upshift (positive delay, as will be shown below) of $3s$ phase points to a slower emergence of the $3s$ electron, while the downshift of $3p$ suggests the opposite.

Until recently, there was an ambiguity about the direction of relative variations between $3p$ and $3s$ phases at their Cooper minima. Schoun *et al.* have measured the variation of argon $3p$

phase for the PR process across the Cooper minima [22]. The correlation phase in the previous calculation was not correct [19]. In the present calculation, this error has been rectified by using the correct sign of the imaginary part of the overall term. Note further in Fig. 2(b) that the $3p \rightarrow ks$ phase is large and rather monotonic as a function of energy, since no Cooper minimum exists in this channel. A crucial consequence of this fact will be recognized in the following.

In streaking experiments, one measures the delay associated with the angle-resolved phase of the *full* $3p$ amplitude of emissions at a solid angle Ω_k [46]. Ignoring the phase of the spherical harmonics, this can be written as

$$\Gamma_{3p}(\Omega_k) = \arg[|D_{3p \rightarrow kd}(\Omega_k)| \exp(i\Gamma_{3p \rightarrow kd}) + |D_{3p \rightarrow ks}(\Omega_k)| \exp(i\Gamma_{3p \rightarrow ks})]. \quad (12)$$

In a non-angle-resolved measurement such as RABITT, the total amplitude is close to the direct sum of the dipole matrix elements $|D|$ over Ω_k in (12). Since for a given channel $\int d\Omega_k |D_{3p \rightarrow kd(s)}(\Omega_k)|^2 \sim \sigma_{3p \rightarrow kd(s)}$, we approximate the integrals over the $|D|$ by the square root of the respective channel cross sections. The TDLDA $3p$ phase is thus calculated by

$$\Gamma_{3p} = \arg[\sqrt{\sigma_{3p \rightarrow kd}} \exp(i\Gamma_{3p \rightarrow kd}) + \sqrt{\sigma_{3p \rightarrow ks}} \exp(i\Gamma_{3p \rightarrow ks})]. \quad (13)$$

In effect, instead of summing the angle-dependent moduli of each channel amplitude, the square root of the sum of their squares is used. Even though the scheme thus neglects the cross terms (interference) among emissions in different directions (by choosing only the self-terms), we show that the results explain the measured $3p$ photorecombination data [22] obtained in RABITT techniques very well.

Now we model Eq. (13) in an approximate form to develop some insights as

$$\Gamma_{3p} \approx \frac{\sqrt{\sigma_{3p \rightarrow kd}}}{S} \Gamma_{3p \rightarrow kd} + \frac{\sqrt{\sigma_{3p \rightarrow ks}}}{S} \Gamma_{3p \rightarrow ks}, \quad (14)$$

where $S = \sqrt{\sigma_{3p \rightarrow kd}} + \sqrt{\sigma_{3p \rightarrow ks}}$. Although, in general, Eq. (14) may have a limited range of validity, as demonstrated in Fig. 3(a), Eqs. (13) and (14) agree numerically almost perfectly for σ and Γ over the current energy range; it was required to fold the $3p \rightarrow ks$ phase onto the range of $0-2\pi$ rad [Fig. 3(a)] before applying (14). The advantage of the form (14) is that it explicitly shows the energy-dependent fractions, the branching strengths, of channel phases in Γ_{3p} . Figure 2(c) presents these branching strengths in Eq. (14) that show the influence of the $3p$ Cooper minimum. Note that the branching strengths should be identical for PI and PR, since the coefficients from detailed balance cancel out in the ratio.

In the following, we compare our TDLDA results for the $3p$ photoelectron with the recently measured absolute $3p$ phase and associated time delay across the $3p$ Cooper minimum in the PR process [22]. Figure 3(a) shows that the $3p \rightarrow kd$ TDLDA phase qualitatively matches the measured phase, albeit with a sharper energy variation for the TDLDA while the measurement shows a softer behavior. However, Eqs. (13) and (14) provide softer variations of the total $3p$ phase around the minimum, which then are in very good agreement with the measurement [22], as seen in Fig. 3(a). Note that the experimental phase was redshifted by 5 eV. It

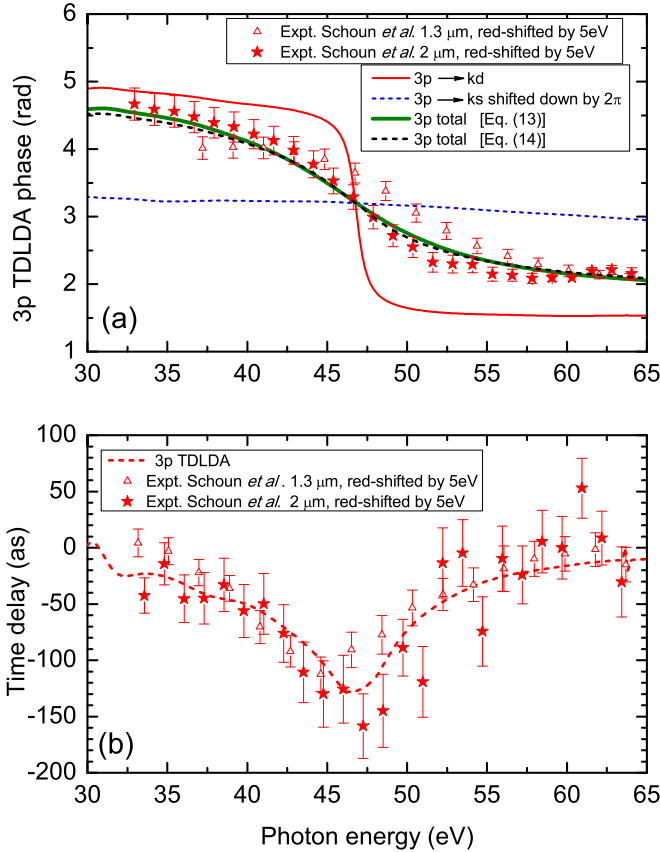


FIG. 3. (Color online) (a) Total 3p TDLDA phase [Eq. (13)] and an admixture [Eq. (14)] of 3p → kd, ks phases (both shown with 3p → ks shifted down by 2π) compared with measured phases for 3p photorecombination [22], but shifted upward by 4 rad. (b) Same as in (a) but for 3p Wigner-Smith time delay. Experimental results are redshifted by 5 eV in both the cases (open triangles, 1.3 μm; stars, 2 μm).

was also necessary to shift the measured data up by 4 rad for comparison. This is because, since the actual observable measured is the derivative of the phase, there is an arbitrary constant shift of the total phase.

Why does the 3p total phase have a considerably softer energy dependence than the 3p → kd phase across the 3p minimum in Fig. 3(a)? This is because, while the 3p → kd channel is generally strong, it becomes very weak near its Cooper minimum so the 3p → ks phase dominates [see Eq. (14)]. Indeed, as evident in Fig. 2(c), while the 3p → kd channel dominates below 40-eV of photon energy, both channels become comparable around 42 eV. With higher energy, this trend continues and enables 3p → ks to eventually contribute about 90% of the total strength right at the Cooper minimum. Past the minimum, however, the 3p → kd channel recovers and regains its dominance above 55 eV. Hence, Eq. (14) makes it explicit that this reversal of relative strengths at the minimum invokes a slower variation of the 3p total phase, retaining its value close to the 3p → kd phase before and after the minimum but producing values close to the (folded) 3p → ks phase near the minimum [Fig. 3(a)].

The energy derivative of the 3p phase, its Wigner-Smith time delay, is performed to calculate the time delay of

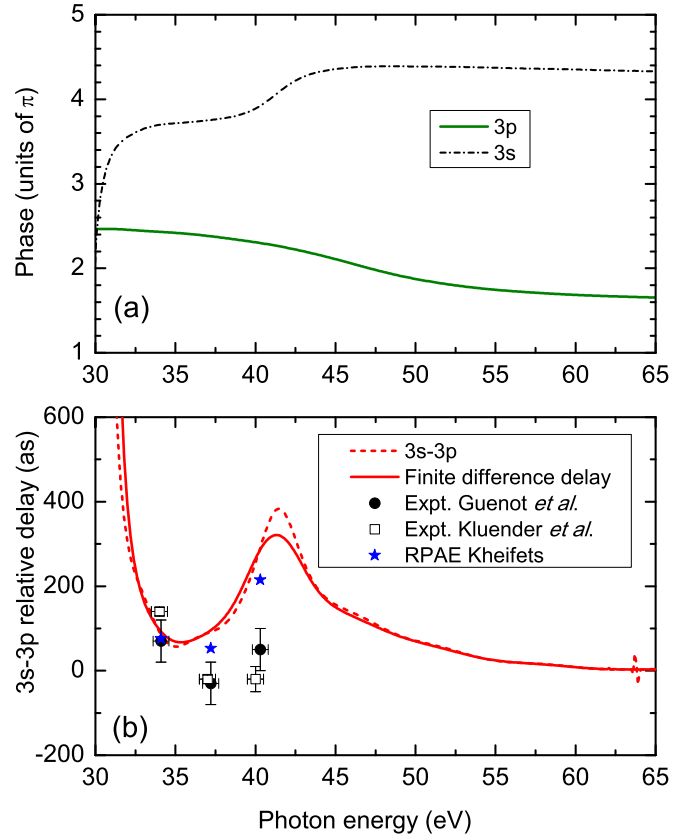


FIG. 4. (Color online) (a) The TDLDA 3s phase and total 3p phase calculated using Eq. (13). (b) The TDLDA relative 3s-3p Wigner-Smith and finite-difference time delays and their comparison with the measured relative delays by the RABITT method (closed circles, Ref. [7]; open squares, Ref. [6]). The RPAE results [18] are also included for comparison.

3p photoelectrons. Respective Wigner-Smith delays for the 3p PR, TDLDA versus experiment, are then compared in Fig. 3(b), which also exhibit nice agreement.

The total 3p phase obtained from (13) is now compared with the TDLDA 3s phase in Fig. 4(a). They show opposite energy gradients in the range from above the 3s Coulomb region near its threshold to energies past the 3p Cooper minimum. The energy differentials of the 3s and 3p phases, their Wigner-Smith time delays, are carried out to calculate the relative time delay between 3s and 3p photoelectrons. Figure 4(b) presents the calculated relative delay in TDLDA and its comparison with the PI measurements [6,7]. The TDLDA and the measured delays are not in good agreement, except at the lowest experimental energy, farthest from the 3s Cooper minimum. We also present the results calculated by the RPAE at the three measured energies [18]. The TDLDA and RPAE results are fairly close and show stronger variations at the 3s Cooper minimum from the structures they predict across the minimum, while the measurements exhibit rather small relative delays. Note, however, that both TDLDA and RPAE predictions and the measurements generally indicate similar qualitative trends (curvatures). We remark that, since, as shown above, the TDLDA agreed so well with the measured 3p delay, measurements of the 3s absolute delay in future, either for the

PI or PR process, may shade lights towards accounting for this theory-experiment quantitative discrepancy in Fig. 4(b).

The RABITT measurement [6,7] used an IR probe pulse of 1.55-eV (800-nm) energy to extract the time delay from measured phases Γ in a finite-difference approach: $\tau(E) = [\Gamma(E + \omega) - \Gamma(E - \omega)]/2\omega$. In order to mimic this experimental procedure, we also apply finite differencing of our TDLDA phases [Fig. 4(a)] using 1.55-eV half steps. Resulting finite difference relative-delay is also presented in Fig. 4(b) which, even though is slightly different from the exact result, does not improve the agreement. We should mention here that we also have calculated the finite-difference TDLDA $3p$ delays with 1.3- μm and 2.0- μm half steps, which are IR photon energies in the PR experiment [22], but obtained virtually the same results of Fig. 3(b).

IV. CONCLUSION

To summarize, a detailed theoretical study of argon valence photoionization and photorecombination spectral phases and associated Wigner-Smith time delays has been carried out within the TDLDA methodology. A notion of interchannel

coupling based on Fano formalism to account for electron correlations was introduced to aid the interpretation of the result and to support the generally accepted consensus that PI is a time-reversal process of PR. Numerical results for the phases reveal structures at respective $3p$ and $3s$ Cooper minima with opposite energy variations, resulting from the correlation based on mutual couplings between $3p$ and $3s$ channels. The TDLDA absolute phase and delay results for $3p$ transition were found to be in very good accord with measured data using HHG plus RABITT. The relative $3s$ - $3p$ Wigner-Smith time delay was computed and found to mostly disagree with recent RABITT measurements, a fact that needs further investigation. As a final remark, TDLDA calculations using explicit corrections for electron self-interactions [43] with a different exchange-correlation functional [47] produced results qualitatively similar to those presented here.

ACKNOWLEDGMENT

The research was supported by the National Science Foundation, USA.

-
- [1] M. Hentschel, R. Kienberger, C. Spielmann, G. A. Reider, N. Milosevic, T. Brabec, P. Corkum, U. Heinzmann, M. Drescher, and F. Krausz, *Nature (London)* **414**, 509 (2001).
- [2] E. Goulielmakis, M. Schultze, M. Hofstetter, V. S. Yakovlev, J. Gagnon, M. Uiberacker, A. L. Aquila, E. M. Gullikson, D. T. Attwood, R. Kienberger, F. Krausz, and U. Kleineberg, *Science* **320**, 1614 (2008).
- [3] P. M. Paul, E. S. Toma, P. Breger, G. Mullot, F. Augé, P. Balcou, H. G. Muller, and P. Agostini, *Science* **292**, 1689 (2001).
- [4] Y. Mairesse, A. De Bohan, L. J. Frasinski, H. Merdji, L. C. Dinu, P. Monchicourt, P. Breger, M. Kovačev, R. Taïeb, B. Carré, H. G. Muller, P. Agostini, and P. Salieres, *Science* **302**, 1540 (2003).
- [5] M. Schultze, M. Fie, N. Karpowicz, J. Gagnon, M. Korbman, M. Hofstetter, S. Neppel, A. L. Cavalieri, Y. Komninos, T. Mercouris, C. A. Nicolaides, R. Pazourek, S. Nagele, J. Feist, J. Burgdörfer, A. M. Azzeer, R. Ernstorfer, R. Kienberger, U. Kleineberg, E. Goulielmakis, F. Krausz, and V. S. Yakovlev, *Science* **328**, 1658 (2010).
- [6] K. Klünder, J. M. Dahlström, M. Gisselbrecht, T. Fordell, M. Swoboda, D. Guénot, P. Johnsson, J. Caillat, J. Mauritsson, A. Maquet, R. Taïeb, and A. L'Huillier, *Phys. Rev. Lett.* **106**, 143002 (2011).
- [7] D. Guénot, K. Klünder, C. L. Arnold, D. Kroon, J. M. Dahlström, M. Miranda, T. Fordell, M. Gisselbrecht, P. Johnsson, J. Mauritsson, E. Lindroth, A. Maquet, R. Taïeb, A. L'Huillier, and A. S. Kheifets, *Phys. Rev. A* **85**, 053424 (2012).
- [8] S. Neppel, R. Ernstorfer, E. M. Bothschafter, A. L. Cavalieri, D. Menzel, J. V. Barth, F. Krausz, R. Kienberger, and P. Feulner, *Phys. Rev. Lett.* **109**, 087401 (2012).
- [9] A. L. Cavalieri, N. Müller, T. Uphues, V. S. Yakovlev, A. Baltuska, B. Horvath, B. Schmidt, L. Blümel, R. Holzwarth, S. Hendel, M. Drescher, U. Kleineberg, P. M. Echenique, R. Kienberger, F. Krausz, and U. Heinzmann, *Nature (London)* **449**, 1029 (2007).
- [10] M. Sabbar, S. Heuser, R. Boge, M. Lucchini, L. Gallmann, C. Cirelli, and U. Keller, [arXiv:1407.6623v1](https://arxiv.org/abs/1407.6623v1).
- [11] D. Guénot, D. Kroon, E. Balogh, E. W. Larsen, M. Kotur, M. Miranda, T. Fordell, P. Johnsson, J. Mauritsson, M. Gisselbrecht, K. Varju, C. L. Arnold, T. Carette, A. S. Kheifets, E. Lindroth, A. L'Huillier, and J. M. Dahlström, *J. Phys. B* **47**, 245602 (2014).
- [12] M. Ivanov and O. Smirnova, *Phys. Rev. Lett.* **107**, 213605 (2011).
- [13] S. Nagele, R. Pazourek, J. Feist, and J. Burgdörfer, *Phys. Rev. A* **85**, 033401 (2012).
- [14] J. M. Dahlström, D. Guénot, K. Klünder, M. Gisselbrecht, J. Mauritsson, A. L'Huillier, A. Maquet, and R. Taïeb, *Chem. Phys.* **414**, 53 (2013).
- [15] E. P. Wigner, *Phys. Rev.* **98**, 145 (1955).
- [16] F. T. Smith, *Phys. Rev.* **118**, 349 (1960).
- [17] J. M. Dahlström, T. Carette, and E. Lindroth, *Phys. Rev. A* **86**, 061402 (2012).
- [18] A. S. Kheifets, *Phys. Rev. A* **87**, 063404 (2013).
- [19] G. Dixit, H. S. Chakraborty, and M. E.-A. Madjet, *Phys. Rev. Lett.* **111**, 203003 (2013).
- [20] J. M. Dahlström and E. Lindroth, *J. Phys. B* **47**, 124012 (2014).
- [21] T. Carette, J. M. Dahlström, L. Argenti, and E. Lindroth, *Phys. Rev. A* **87**, 023420 (2013).
- [22] S. B. Schoun, R. Chirla, J. Wheeler, C. Roedig, P. Agostini, L. F. DiMauro, K. J. Schafer, and M. B. Gaarde, *Phys. Rev. Lett.* **112**, 153001 (2014).
- [23] H. J. Wörner, H. Niikura, J. B. Bertrand, P. B. Corkum, and D. M. Villeneuve, *Phys. Rev. Lett.* **102**, 103901 (2009).
- [24] J. Higué, H. Ruf, N. Thiré, R. Cireasa, E. Constant, E. Cormier, D. Descamps, E. Mével, S. Petit, B. Pons, Y. Mairesse, and B. Fabre, *Phys. Rev. A* **83**, 053401 (2011).

- [25] J. P. Farrell, L. S. Spector, B. K. McFarland, P. H. Bucksbaum, M. Gühr, M. B. Gaarde, and K. J. Schafer, *Phys. Rev. A* **83**, 023420 (2011).
- [26] A. D. Shiner, B. E. Schmidt, C. Trallero-Herrero, P. B. Corkum, J. C. Kieffer, F. Légaré, and D. M. Villeneuve, *J. Phys. B* **45**, 074010 (2012).
- [27] J. B. Bertrand, H. J. Wörner, P. Hockett, D. M. Villeneuve, and P. B. Corkum, *Phys. Rev. Lett.* **109**, 143001 (2012).
- [28] M. C. H. Wong, A. T. Le, A. F. Alharbi, A. E. Boguslavskiy, R. R. Lucchese, J. P. Brichta, C. D. Lin, and V. R. Bhardwaj, *Phys. Rev. Lett.* **110**, 033006 (2013).
- [29] L. D. Landau and E. M. Lifshitz, *Quantum Mechanics: Non-relativistic Theory* (Pergamon, New York, 1965).
- [30] T. Morishita, A.-T. Le, Z. Chen, and C. D. Lin, *Phys. Rev. Lett.* **100**, 013903 (2008).
- [31] A.-T. Le, R. R. Lucchese, S. Tonzani, T. Morishita, and C. D. Lin, *Phys. Rev. A* **80**, 013401 (2009).
- [32] B. Möbus, B. Magel, K. H. Schartner, B. Langer, U. Becker, M. Wildberger, and H. Schmoranzner, *Phys. Rev. A* **47**, 3888 (1993).
- [33] J. A. R. Samson and W. C. Stolte, *J. Electron Spectrosc. Relat. Phenom.* **123**, 265 (2002).
- [34] T. Barillot, C. Cauchy, P.-A. Hervieux, M. Gisselbrecht, S. E. Canton, P. Johnsson, J. Laksman, E. P. Mansson, J. M. Dahlström, M. Magrakvelidze, G. Dixit, M. E. Madjet, H. S. Chakraborty, E. Suraud, P. M. Dinh, P. Wopperer, K. Hansen, V. Lorient, C. Bordas, S. Sorensen, and F. Lépine, *Phys. Rev. A* **91**, 033413 (2015).
- [35] M. Magrakvelidze, D. M. Anstine, G. Dixit, M. E.-A. Madjet, and H. S. Chakraborty, *Phys. Rev. A* **91**, 053407 (2015).
- [36] M. E. Madjet, H. S. Chakraborty, and J.-M. Rost, *J. Phys. B* **34**, L345 (2001).
- [37] A. Zangwill and P. Soven, *Phys. Rev. A* **21**, 1561 (1980).
- [38] M. Stener, G. De Alti, G. Fronzoni, and P. Decleva, *Chem. Phys.* **222**, 197 (1997).
- [39] R. van Leeuwen and E. J. Baerends, *Phys. Rev. A* **49**, 2421 (1994).
- [40] D. J. Kennedy and S. T. Manson, *Phys. Rev. A* **5**, 227 (1972).
- [41] W. Ekardt, *Phys. Rev. B* **31**, 6360 (1985).
- [42] T. Nakatsukasa and K. Yabana, *J. Chem. Phys.* **114**, 2550 (2001).
- [43] M. E. Madjet, H. S. Chakraborty, J. M. Rost, and S. T. Manson, *J. Phys. B* **41**, 105101 (2008).
- [44] U. Fano, *Phys. Rev.* **124**, 1866 (1961).
- [45] Since RABITT experiments cannot resolve s and d channels, the coupling between $3p \leftrightarrow ks$ and $3s \leftrightarrow kp$ also contributes, but only quantitatively.
- [46] J. Wätzel, A. S. Moskalenko, Y. Pavlyukh, and J. Berakdar, *J. Phys. B* **48**, 025602 (2015).
- [47] O. Gunnerson and B. Lundqvist, *Phys. Rev. B* **13**, 4274 (1976).